Pediatr Radiol (2012) 42:1347–1356
DOI 10.1007/s00247-012-2444-9

ORIGINAL ARTICLE

An MRI system for imaging neonates in the NICU: initial feasibility study

Jean A. Tkach · Noah H. Hillman · Alan H. Jobe · Wolfgang Loew · Ron G. Pratt · Barret R. Daniels · Suhas G. Kallapur · Beth M. Kline-Fath · Stephanie L. Merhar · Randy O. Giaquinto · Patrick M. Winter · Yu Li · Machiko Ikegami · Jeffrey A. Whitsett · Charles L. Dumoulin

Received: 6 February 2012 / Revised: 9 May 2012 / Accepted: 17 May 2012 / Published online: 27 June 2012

Abstract
Background Transporting premature infants from a neonatal intensive care unit (NICU) to a radiology department for MRI has medical risks and logistical challenges.
Objective To develop a small 1.5-T MRI system for neonatal imaging that can be easily installed in the NICU and to evaluate its performance using a sheep model of human prematurity.
Materials and methods A 1.5-T MRI system designed for orthopedic use was adapted for neonatal imaging. The system was used for MRI examinations of the brain, chest and abdomen in 12 premature lambs during the first hours of life. Spin-echo, fast spin-echo and gradient-echo MR images were evaluated by two pediatric radiologists.
Results All animals remained physiologically stable throughout the imaging sessions. Animals were imaged at two or three time points. Seven brain MRI examinations were performed in seven different animals, 23 chest examinations in 12 animals and 19 abdominal examinations in 11 animals. At each anatomical location, high-quality images demonstrating good spatial resolution, signal-to-noise ratio and tissue contrast were routinely obtained within 30 min using standard clinical protocols.
Conclusion Our preliminary experience demonstrates the feasibility and potential of the neonatal MRI system to provide state-of-the-art MRI capabilities within the NICU. Advantages include overall reduced cost and site demands, lower acoustic noise, improved ease of access and reduced medical risk to the neonate.

Keywords Neonatal MRI · NICU · MRI · Prematurity

J. A. Tkach (✉) · W. Loew · R. G. Pratt · B. R. Daniels · R. O. Giaquinto · P. M. Winter · Y. Li · C. L. Dumoulin
Imaging Research Center, Department of Radiology,
Cincinnati Children's Hospital Medical Center,
3333 Burnet Ave., MLC 5033, Cincinnati, OH 45229, USA
e-mail: jean.tkach@cchmc.org

J. A. Tkach · W. Loew · R. G. Pratt · B. R. Daniels · B. M. Kline-Fath · R. O. Giaquinto · P. M. Winter · Y. Li · C. L. Dumoulin
Department of Radiology,
Cincinnati Children's Hospital Medical Center,
Cincinnati, OH, USA

N. H. Hillman · A. H. Jobe · S. G. Kallapur · S. L. Merhar · M. Ikegami · J. A. Whitsett
Division of Neonatology and Pulmonary Biology,
Perinatal Institute, Cincinnati Children's Hospital Medical Center,
Cincinnati, OH, USA

Introduction

While MRI has become an important and powerful diagnostic tool in adult and pediatric radiology, its potential for diagnosing disease in premature babies is not fully realized. The few neonates receiving MRI today are typically transported from the NICU to the main radiology department and scanned in an adult-size MRI system [1–6]. MRI-compatible incubators with integrated radiofrequency (RF) coils have been developed and are commercially available, but their use requires that NICU staff accompany the neonate out of the NICU [4–14]. Even with MRI-compatible incubators, the medical risk involved in the transport of babies typically precludes the smallest and sickest infants from receiving MRI examinations. In addition, image quality, that is signal-to-noise (S/N) ratio and spatial resolution for a given scan time, is compromised by the size mismatch between the neonate and the adult-size scanner and lack of RF coils of appropriate size.

In the late 1990s, a group at Hammersmith Hospital in London together with Oxford Magnet Technology (Eynsham, UK) and Marconi (Picker) International (Cleveland, OH), brought MRI to the baby by installing a 1.0-T system developed specifically for the neonate in the NICU. This system was primarily utilized for cranial MRI and MR spectroscopy (MRS) in premature infants [7]. The scanner had several undesirable characteristics, including a limited field of view (FOV) and a 2-T fringe field, and has since been replaced by a conventional 3-T MRI scanner [8]. Unfortunately, the use of an adult-size MRI system retains the disadvantages associated with the size mismatch between the neonate and the scanner and the relatively long bore length limits visual and rapid physical access to the neonate during the examination. Also, the safety risks associated with ferromagnetic objects in the scan room are greater at the higher field strength and with an adult-size magnet bore [4]. In addition, an increased risk of tissue heating (specific absorption rate increases fourfold as magnetic field strength is doubled from 1.5 T to 3.0 T) and limited availability of MRI-compatible equipment are concerns at the higher field strength. A group in Sheffield, UK, has addressed these concerns by installing a small customized low-field (0.17 T) MRI system (InnerVision MRI, London, UK) in the NICU at their institution [9]. However, the types and sophistication of the MRI acquisitions that can be performed on this system are severely limited by the inherently lower S/N ratio at 0.17 T.

Results from these institutions and others have shown that MRI and MRS do in fact have substantial potential benefits for neonatal medicine [5–7, 10–38]. However, the most significant barrier to the extensive use of MRI in neonatology is the challenge associated with examination logistics. We report our experience with the development of a dedicated small-footprint, high field strength neonatal MRI unit that has been installed in a preclinical imaging research laboratory at our institution and the results of the initial imaging studies performed in a lamb model of human prematurity. The imaging data collected were used to assess the efficacy and potential of this platform for human neonatal MRI. The data presented here have justified the installation of another small-bore MRI system with the identical configuration in our institution's NICU. This second system is now being used to perform clinical neonatal MRI examinations.

Materials and methods

Neonatal MRI system

We have adapted a small 1.5-T MRI system designed for orthopedic applications and originally developed and marketed as the MSK Extreme 1.5 T by ONI Medical Systems (Wilmington, MA). Recently, GE purchased ONI, and the scanner is now being marketed as the OPTIMA MR430s (GE Healthcare, Waukesha, WI) and is referred to as such in the remainder of this article. Several modifications to the OPTIMA scanner were made to accommodate neonatal imaging. Specifically, the orientation and height of the magnet were changed (Fig. 1) and the patient chair was replaced with a custom-built MRI patient table. The magnet is superconducting and has a field strength of 1.5 T. The scanner has a maximum patient bore diameter of 21.8 cm (without RF coil) and roughly twice the gradient strength (70 mT/m) and slew rate (300 T/m/s) of the best conventional adult whole-body systems. Unlike the majority of adult-size commercial scanners, the OPTIMA system does not have a fixed RF body coil. Single-channel transmit/receive volume coils with inner diameters of 180 mm, 160 mm, 145 mm, 123 mm, 100 mm and 80 mm are delivered with the system for imaging. A comparison of the specifications of the OPTIMA and a conventional GE HDx whole-body 1.5-T scanner is provided in Table 1. The salient differences between the systems include

Fig. 1 Photograph of the 1.5-T OPTIMA MRI system after modification for neonatal imaging. Modifications to the OPTIMA system at the time of the sheep studies included increasing the magnet height and leveling to true horizontal. Additional modifications made subsequent to the sheep studies included: (1) replacing the chair used to support the patient for extremity scanning by a customized patient table, and (2) integration of the measurement control electronics, RF chain and system operating software of a state-of-the-art 1.5-T adult-size scanner with the basic OPTIMA system to enable the full spectrum of advanced imaging capabilities. At present, two enhanced neonatal MRI units are installed and in operation at our institution. One system is located in the Imaging Research Center and is being used for preclinical research (such as the initial preterm sheep study). The second neonatal MRI system is located in the NICU and is being used to perform patient examinations and clinical research studies

Table 1 MRI system specification comparison: conventional (1.5-T HDx GE) and NICU (1.5-T OPTIMA MR430) MRI systems

System characteristic	Conventional system	NICU system
Field strength (T)	1.5, active shielded	1.5, active shielded
Magnet type	Superconducting, active and passive shims	Superconducting, passive shims
Fringe field (5-G line) (m)	4.0×2.5 (axial × radial)	1.85×1.125 (axial × radial)
Bore (cm)		
Internal diameter	60 (with body RF coil)	21.8 (without RF coil)
Length[a]	90	51.8
Magnet weight (with cryogens and gradient coil)	12,170 lbs (5,532 kg)	Magnet <900 lbs (408 kg); compressor weight 203 lbs (92 kg)
Field stability (ppm/h)	<0.1	0.1
Helium capacity (l)	2,000 (nominal) liquid helium	49 (nominal) liquid helium
Helium refills	Approximately every 4 years	Typically not required
Gradient		
Strength (mT/m)	30	70
Slew rate (T/m/s)	120	300
RF transmit/receive		
Frequency	63.8 MHz±600 kHz	63.8 MHz±63.8 kHz
Power	21 kW (body), 4 kW (head)	2 kW peak RMS, 75 W average
Acoustic noise (dBA)[b]		
Average	97.5±2.9	86.2±2.6
Worst case	103 (DWI)	91 (SSFP)

[a] Not including the flare from the end of the magnet.

[b] Acoustic noise measurements reported here were made as part of this study.

patient bore diameter, location of the 5-G line, magnet weight, cryogen requirements and gradient performance. Magnet room RF shielding and air temperature and humidity requirements for the neonatal scanner are identical to those required for adult-size MRI systems. It is important to note that despite the superior gradient performance afforded by the smaller gradient RF coils, acoustic noise and the potential for peripheral nerve stimulation are less than that of conventional adult-size MRI scanners. Vital signs (e.g., ECG, oxygen saturation, body temperature, respiration) are monitored during scanning using MRI-compatible equipment.

The technical performance of the NICU MRI unit was evaluated and compared with that of a state-of-the-art adult-size 1.5-T whole-body MRI scanner. Identical imaging protocols were used to collect axial spin-echo images of a standard phantom with both the neonatal MRI scanner and a conventional adult-size whole-body 1.5-T HDx GE MRI system (GE Healthcare, Waukesha, WI) using RF coils of similar volume. The images were evaluated for S/N ratio, geometric accuracy/fidelity and spatial resolution. S/N ratio measurements were obtained by dividing the mean signal intensity of a 730-mm^2 circular region of interest placed at the center of a homogeneous portion of the phantom by the standard deviation of the noise measured for a circular region of interest of identical size placed outside the phantom. Geometric fidelity was assessed by measuring the inner diameter of the phantom at identical slice locations for both scanners and comparing the measured values against the known dimension reported by the phantom manufacturer. Spatial resolution was evaluated by the ability to clearly resolve 3-mm spaced line pairs.

The inherent acoustic noise characteristics of the NICU MRI scanner were evaluated with sound pressure level (SPL) measurements and compared to those from a conventional adult-size whole-body 1.5-T HDx GE MRI system with the sensor placed at the iso-center of both units. A sound level meter (model 2250; Brüel & Kjær Sound & Vibration Measurement, Nærum, Denmark) was used to measure the SPL for six different standard MRI acquisitions using clinically relevant parameters: spin-echo, gradient-echo, fast RF spoiled gradient-echo, echo-planar, fully balanced steady-state free precession (SSFP), and diffusion-weighted imaging (DWI). The MRI sequences, acquisition parameters, noise measurement equipment and methodology were identical for the two systems. The average SPL in units of A-weighted decibels was recorded for each of the MRI acquisition/MRI system combinations evaluated. The SPL in units of decibels as a function of frequency over the range of 50–20,000 Hz was also documented for each MRI acquisition/MRI system tested.

Animal model

Animal MRI studies were performed on the preterm twin lambs of six ewes during their first 7 h of life. The animal protocol was approved by the Institutional Animal Care and Use Committee (IACUC) at our institution. The six sets of preterm twin sheep were delivered by caesarean section at 129–132 days' gestational age from the ventilated ewe under general anesthesia with 20 mg/kg ketamine (Fort Dodge Animal Health, Fort Dodge, IA) plus 0.1 mg/kg intramuscular xylazine (Lloyd Laboratories, Shenandoah, IA) and spinal/epidural anesthesia with 8 ml 2% lidocaine (Hospira, Lake Forest, IL). The average birth weight was 3.3±0.3 kg. The fetal head and chest were exposed. The lamb was anesthetized with 10 mg/kg ketamine or 0.1 mg/kg intramuscular xylazine, and 2% lidocaine was injected subcutaneously to the neck for tracheostomy. Because preterm lambs at this gestational age require surfactant treatment to survive, each was treated with surfactant (Curosurf 100 mg/kg; Chiesi Farmaceutici, Italy) through the tracheostomy tube and ventilated with 30 cmH_2O peak inspiratory pressure (PIP) and 4 cmH_2O peak-positive end-expiratory pressure (PEEP). Each newborn lamb was then covered with plastic wrap to maintain body temperature, ventilated using a pressure-limited infant ventilator (Sechrist Industries, Anaheim, CA), and transferred to the imaging suite for the MRI examination. Ventilation was maintained uninterrupted throughout the 7-h imaging session.

Physiological monitoring

The lambs received the same monitoring as human preterm infants in the NICU, with special attention paid to heart rate, blood pressure, oxygen saturation, respiration and body temperature. Continuous hemodynamic monitoring was accomplished using a 3150 MRI Patient Monitoring System (InVivo, Gainesville, FL). Measurements of physiological parameters, including body temperature, blood gas, pH, hematocrit, glucose, tidal volume, PIP and PEEP were made hourly. To help maintain body temperature, the animals remained covered in plastic wrap for the duration of the 7-h imaging session. In addition, during scanning, the animals were placed on a pad attached to a heated circulating water bath, maintained at 37°C. The animals were placed on a standard warming bed (Ohio NC Neonatal Care Unit; Ohio Medical Corporation, Madison, WI) positioned inside the scan room to maintain body temperature when they were not being imaged.

MRI acquisition

Two animals were evaluated in each 7-h imaging session (six sessions in total). Each animal was imaged at two or three time points during the 7-h period. The earliest imaging time point began approximately 30 min after delivery, and the final images were obtained approximately 6.5 h after delivery.

The duration of the MRI scan performed at each time point ranged from 30 min to 60 min. Imaging was performed with a 14.5-cm volume RF coil. The brain, chest and abdomen were evaluated using conventional MRI spin-echo, fast spin-echo and gradient-echo sequences. Some advanced MRI techniques such as DWI (a mainstay of neonatal brain MRI examinations) are not supported by the basic OPTIMA system and therefore were not available at the time of the preterm sheep studies. The brain was only evaluated once for each animal during the 7-h time period since ischemic changes were not expected on the standard MRI sequences. However, MRI observable changes were anticipated in the lungs and gastrointestinal (GI) tract during the first few hours of life (i.e., clearance of interstitial fluid from the lungs, and amniotic fluid and meconium from the GI tract). For this reason, the chest and abdomen were imaged at multiple time points for each animal. For each anatomical location, the MRI acquisition parameters (i.e., TR and TE) were selected to produce images exhibiting proton density and T1-weighted, T2-weighted and T2*-weighted tissue contrasts. One or two anatomical locations were evaluated by MRI at each time point. ECG and respiratory gating and triggering were not available at the time of these imaging studies. Spatial presaturation RF pulses were not used in any of the acquisitions.

Image evaluation

The quality of the MR images based on S/N ratio, contrast-to-noise ratio, motion artifact and uniformity, was evaluated subjectively by two experienced board-certified pediatric radiologists. Any incidental abnormal findings (e.g., atelectasis) were also noted.

Fig. 2 Axial conventional spin-echo images of a standard S/N and spatial resolution phantom acquired on the OPTIMA MRI scanner demonstrate accurate geometric dimensions and good spatial resolution. Acquisition parameters: TR 500 ms, TE 14 ms, FOV 160 mm, matrix 256×256, slice thickness 5 mm, receiver bandwidth 32 kHz, number of acquisitions 1, scan time 2 min 8 s

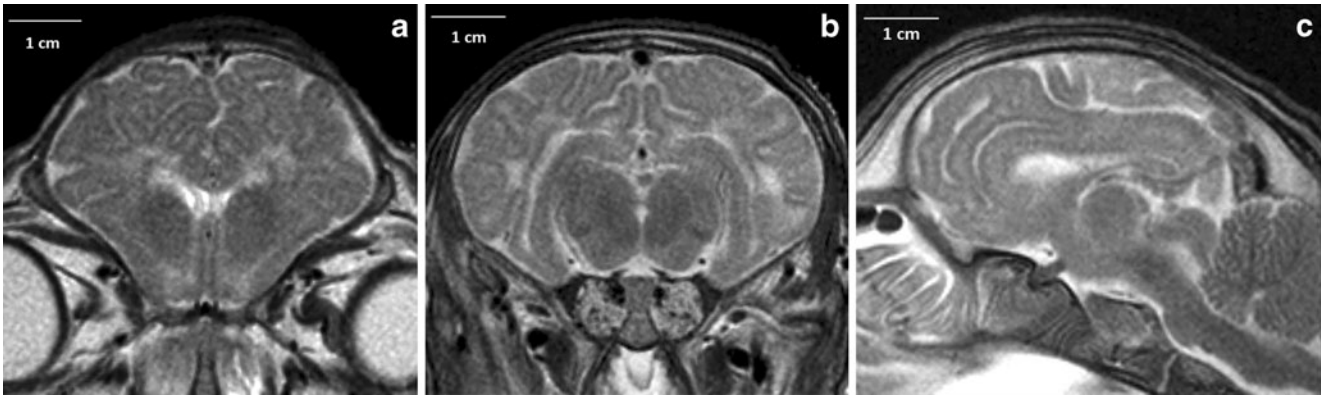

Fig. 3 Fast spin-echo T2-weighted images of the neonatal sheep brain demonstrate a small FOV, high in-plane spatial resolution (0.35 mm× 0.35 mm) and excellent tissue contrast. Acquisition parameters for (**a**) and (**b**): TR 3,000 ms, TE 120 ms, FOV 90 mm, matrix 256×256, slice thickness 2 mm, echo train length 12, receiver bandwidth 50 kHz, number of acquisitions 5, scan time 5 min 20 s. Acquisition parameters for (**c**): identical except for TR 4,000 ms, number of acquisitions 4, scan time 5 min 41 s

Results

NICU MRI system performance

The S/N ratio of the NICU MRI system was comparable to that of the state-of-the-art adult-size 1.5-T scanner (S/N 735 for the NICU MRI vs. S/N 664 for the conventional 1.5-T GE HDx). The phantom images demonstrated accurate geometric fidelity and spatial resolution (Fig. 2).

Acoustic noise

The maximum SPL values measured for the NICU MRI during each of the six MRI acquisitions were consistently lower (range 5–18 dBA) than those for the conventional adult-size MRI scanner. The average measured SPL value across all acquisitions as well as the SPL values for the worst-case acquisitions are reported in the final rows of Table 1. For the NICU MRI system, the highest SPL value (91 dBA, compared to 96 dBA for the HDx GE system) was measured for the SSFP sequence. Alternatively, for the HDx GE MRI system, the highest SPL value (103 dBA, compared to 85 dBA for the NICU MRI system) was measured for the DWI sequence. The measured SPL as a function of frequency showed a similar harmonic structure above 200 Hz between the MRI systems for all sequences, albeit with lower amplitudes for the smaller gradient coil. The larger gradient coils of the HDx system were substantially louder (as much as 30 dB) at frequencies below 200 Hz.

Animals

All 12 lambs were maintained well on the ventilator, with a stable mean arterial pressure of 45±5 mmHg, a heart rate of 143±6 bpm, a temperature of 37±0.5°C, a PaO_2 of 87±20 mmHg and a $PaCO_2$ of 52±6 mmHg.

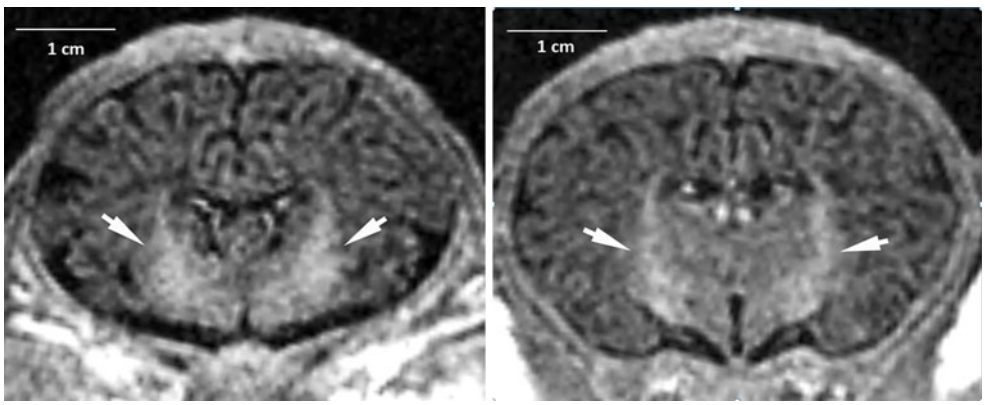

Fig. 4 T1-weighted fast spin-echo inversion recovery images of the neonatal sheep brain demonstrate increased signal in regions of myelination (*arrows*). Acquisition parameters: TR 2,200 ms, TI 750 ms, TE 6.8 ms, FOV 145 mm, matrix 256×256, slice thickness 2 mm, voxel size 0.57×0.57 mm in-plane and 2 mm through-plane, echo train length 4, receiver bandwidth 65 kHz, number of acquisitions 2, scan time 4 min 42 s

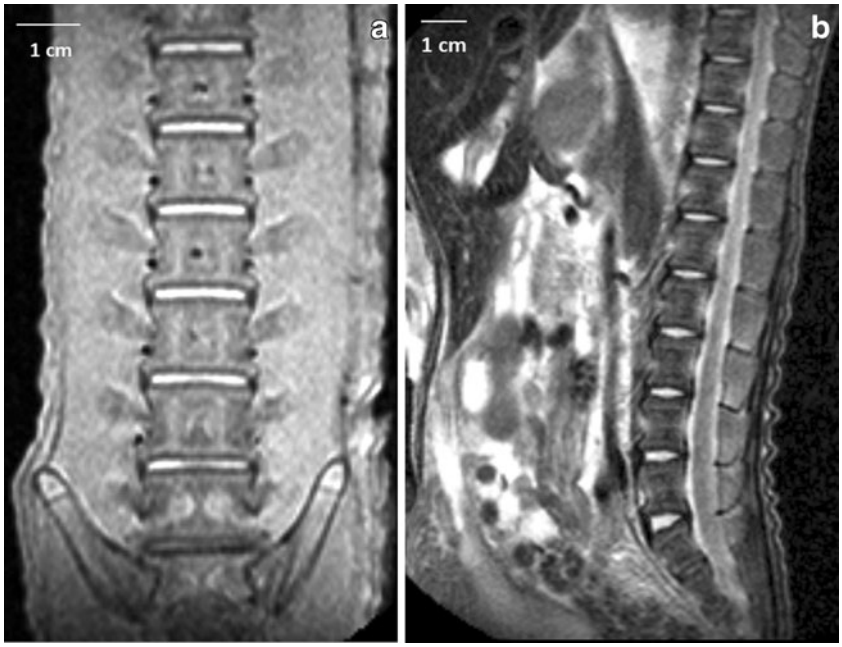

Fig. 5 Coronal spin density (**a**) and sagittal T2-weighted (**b**) images of the spine. No anterior saturation pulse was applied. Acquisition parameters: **a** fast spin-echo inversion recovery, TR 4,000 ms, TI 155 ms, TE 7.5 ms, FOV 145 mm, matrix 192×256, slice thickness 3.5 mm, voxel size 0.76×0.57 mm in-plane and 3.5 mm through-plane, echo train length 6, receiver bandwidth 50 kHz, number of acquisitions 2, scan time 4 min 16 s; **b** fast spin-echo, TR 4,000 ms, TE 120 ms, FOV 145 mm, matrix 256×256, slice thickness 3 mm, voxel size 0.57×0.57 mm in-plane and 3 mm through-plane, echo train length 12, receiver bandwidth 50 kHz, number of acquisitions 2, scan time 4 min 16 s

MRI examination

Each of the 12 animals was imaged at two or three time points, typically 1–1.5 h apart. The study protocol limited the total time available for the imaging, and in a few animals the examination had to be terminated before the entire scanning protocol was complete. Seven brain MRI examinations were performed in seven animals, 23 chest examinations in 12 animals and 19 abdominal examinations in 11 animals. High-quality datasets, with a small FOV demonstrating high spatial resolution, and good S/N ratio and tissue contrast, were obtained for all imaging planes at each anatomical location. Five or six datasets, using imaging parameters consistent with standard clinical protocols, were routinely acquired within a scan time of approximately 30 min. Representative images are provided in Figs. 3, 4, 5, 6, 7, 8 and 9.

Brain and spine

In all seven lambs in which brain MRI examinations were performed, T2-W fast spin-echo acquisitions produced images of the brain with a small FOV, high spatial resolution (0.35 mm×0.35 mm in-plane and 2 mm through-plane) demonstrating good contrast between the gray and white matter in

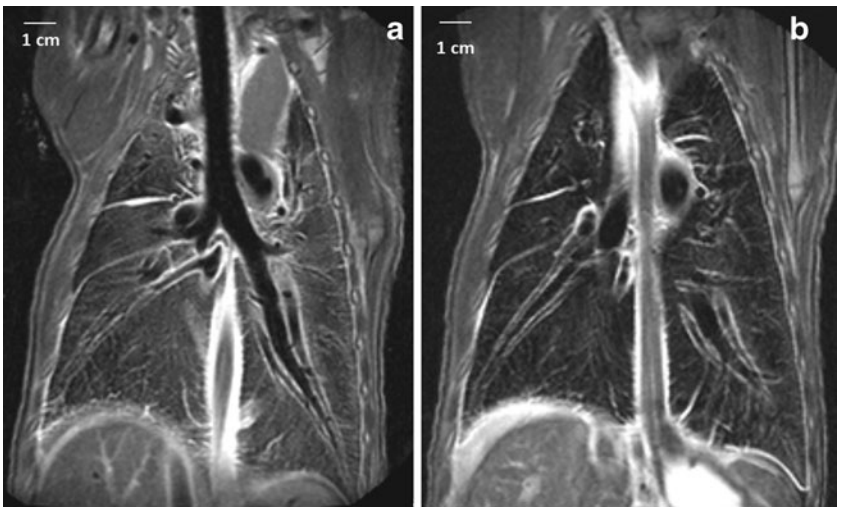

Fig. 6 Coronal T2-weighted images of the lungs in the same animal acquired 3 h (**a**) and 6.5 h (**b**) postpartum show decreasing pulmonary parenchymal signal and interstitial markings, indicating the gradual elimination of fluid from the interstitial space of the lungs during the first few hours of life. Acquisition parameters: fast spin-echo, TR 3,000 ms, TE 81 ms, FOV 145 mm, matrix 256×256, slice thickness 3 mm, voxel size 0.57×0.57 mm in-plane and 3 mm through-plane, echo train length 8, receiver bandwidth 50 kHz, number of acquisitions 4, scan time 6 min 24 s. The window and level settings are the same for both images

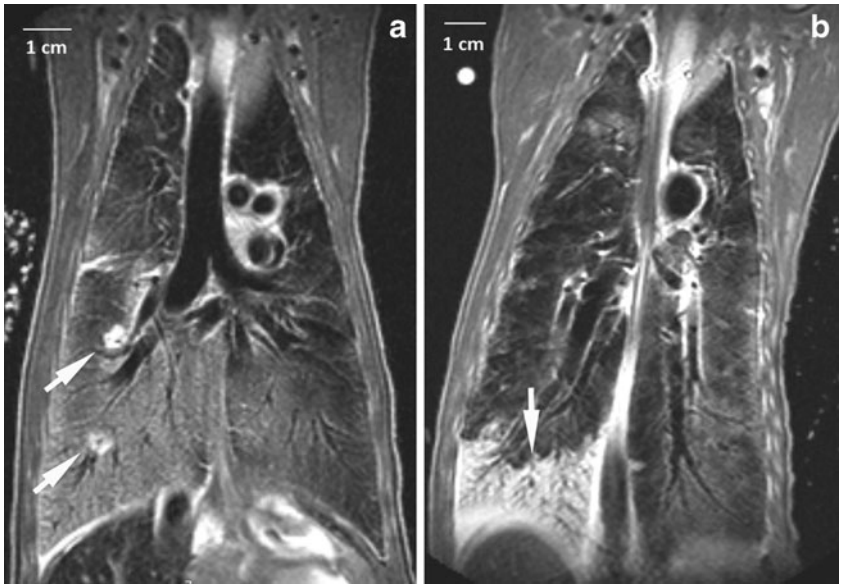

Fig. 7 Coronal T2-weighted images of the lungs of two animals demonstrate areas of parenchymal atelectasis (*arrows*). Acquisition parameters: fast spin-echo, TR 3,000 ms, TE 81 ms, FOV 145 mm, matrix 256×256, slice thickness 3 mm, voxel size 0.57×0.57 mm in-plane and 3 mm through-plane, echo train length 8, receiver bandwidth 50 kHz, number of acquisitions 4, scan time 6 min 24 s

clinically acceptable scan times (Fig. 3). For example, 24 and 36 2-mm T2-W fast spin-echo images of the brain with high spatial resolution could be obtained in scan times of 5 min 20 s and 5 min 41 s, respectively. Regions of early myelination in the brain were well visualized on T1-weighted fast spin-echo inversion recovery images, allowing definition of the immature white matter tracts (Fig. 4). Spine images showed excellent tissue contrast and high spatial resolution (Fig. 5).

Chest

High-resolution images of the lungs and heart were obtained in all 12 animals. The major chambers and vessels of the heart were clearly visualized in all animals, and the pulmonary vasculature, trachea and main bronchi of the lungs were well visualized. Figure 6 shows a pair of images acquired 3.5 h apart in the same animal, demonstrating the gradual clearance of fluid from the interstitial space of the lungs during the first few hours of life. Lung images (Fig. 7) acquired in two animals demonstrated regions of parenchymal atelectasis, illustrating the diagnostic potential of MRI in evaluating preterm pulmonary disease.

Abdomen

The presence of meconium (hyperintense on T1-weighted images) in the GI tract after delivery made it possible to consistently obtain high-quality images of the bowel

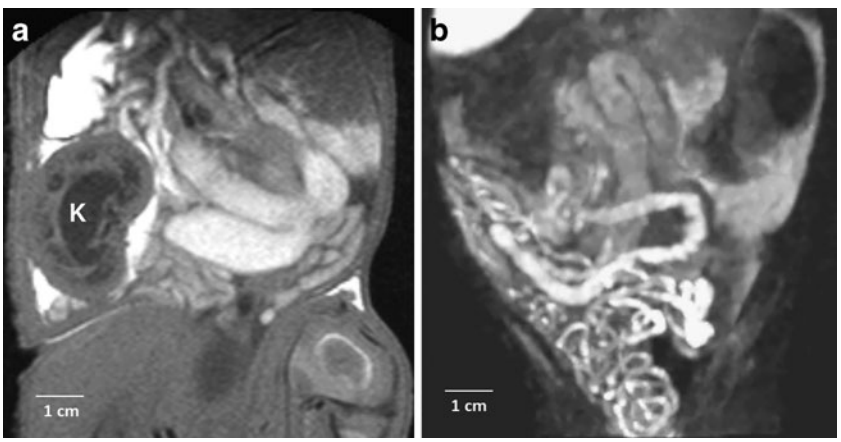

Fig. 8 Abdominal images acquired during the first few hours of life. The presence of intraluminal amniotic fluid and meconium allows excellent visualization of GI anatomy. **a** Coronal T1-weighted spin-echo image of the abdomen. Acquisition parameters: spin-echo, TR 400 ms, TE 12.2 ms, FOV 145 mm, matrix 192×256, slice thickness 3.5 mm, voxel size 0.76×0.57 mm in-plane and 3.5 mm through-plane, echo train length 1, receiver bandwidth 50 kHz, number of acquisitions 3, scan time 3 min 50 s (*K* kidney). **b** Coronal maximum-intensity projection reconstruction of the bowel generated from a 3-D gradient echo dataset. Acquisition parameters: RF spoiled T1-weighted gradient echo, TR 30 ms, TE 4 ms, flip angle 60°, FOV 145 mm, matrix 180×256, 60 2-mm partitions, voxel size 0. 52×0.57 mm in-plane and 2 mm through-plane, receiver bandwidth 50 kHz, number of acquisitions 1, scan time 5 min 24 s

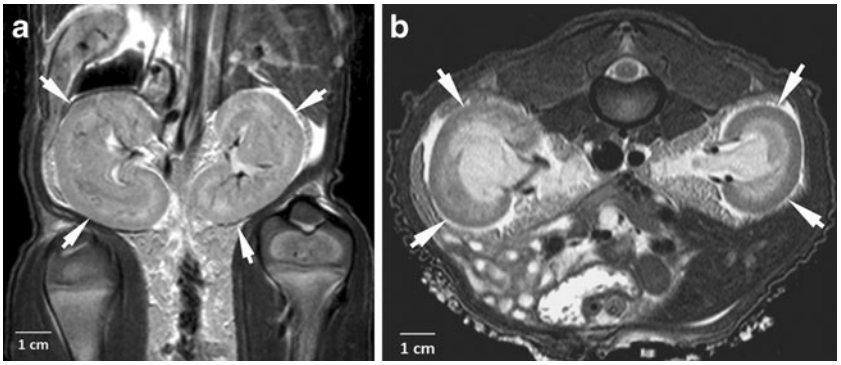

Fig. 9 Coronal (**a**) and axial (**b**) images of the kidneys (*arrows*) show high spatial resolution and excellent tissue contrast. **a** Fast spin-echo, TR 3,000 ms, TE 81 ms, FOV 145 mm, matrix 256×256, slice thickness 3 mm, voxel size 0.57×0.57 mm in-plane and 3 mm through-plane, echo train length 8, receiver bandwidth 50 kHz, number of acquisitions 4, scan time 6 min 24 s. **b** Fast spin-echo, TR 4,000 ms, TE 120 ms, FOV 145 mm, matrix 256×384, slice thickness 2.5 mm, voxel size 0.57×0.38 mm in-plane and 2.5 mm through-plane, echo train length 12, receiver bandwidth 50 kHz, number of acquisitions 3, scan time 4 min 16 s

(Fig. 8). In addition, by reformatting the volumetric MRI data, it was possible to produce a 3-D visualization of the GI tract (Fig. 8). High spatial resolution renal imaging (e.g., voxel size 0.57 mm×0.38 mm in-plane and 2.5 mm through-plane, and 0.53 mm×0.53 mm in-plane and 3 mm through-plane) clearly delineated the cortex and medulla in 4 to 6 min (Fig. 9).

Discussion

The major challenges to the adoption of MRI for everyday clinical use in neonatal medicine include the logistical challenges and medical risks associated with transportation of the infant from the NICU to the main radiology department for the examination [4–6]. In addition, the size mismatch between the neonate and the adult-size RF coils has a negative impact on the image quality (i.e. S/N ratio and spatial resolution). These obstacles are for the most part mitigated by the installation of a small-footprint MRI system in the NICU. Elimination of the logistical challenges of moving a baby out of the NICU greatly reduces the MRI-associated medical risks to the neonate. Although these risks are minimized by physically locating the MRI system within the NICU, the challenges of supporting thermally unstable neonates during the MRI examination remain. For imaging outside the NICU, MRI-compatible incubators are used in these instances [4–14]. However, these devices are costly and require coordinated effort and experience to use. Although we did not use such a system in the preclinical studies reported here, we anticipate reporting the development and use of an MRI-compatible thermal management system for neonatal MRI in a subsequent report.

The neonatal MRI system has several advantages over conventional MRI systems. For example, the small neonatal MRI system is less expensive to purchase and operate. The lower weight, size, fringe field and acoustic noise make it feasible for this system to be placed within a NICU. Another important benefit of the scanner's small size is the concurrent improvement in gradient performance and reduced acoustic noise. The enhanced gradient capabilities of the neonatal MRI system enable a small FOV with high spatial resolution to be obtained without compromising acquisition parameters such as TR and TE for all MRI sequences; these capabilities also allow short inter-echo spacing to be achieved for fast spin-echo and echo-planar imaging acquisitions. The increased gradient performance also benefits phase-contrast and DWI imaging. For example, with phase-contrast MRI, greater sensitivity to velocity is possible. For DWI imaging, higher b-values for a given TE and shorter TE values for a given b-value can be realized.

Since the completion of the initial set of sheep imaging studies, the measurement control electronics of a state-of-the-art 1.5-T GE scanner have been integrated with the basic OPTIMA MRI system. The end result is a dedicated NICU scanner with all of the imaging capabilities of a high-end adult-size 1.5-T MRI system. The enhanced NICU MRI platform supports the full spectrum of advanced imaging techniques (e.g., MRS, diffusion tensor imaging, functional MRI, arterial spin labeling and phase-contrast imaging) as well as ECG and respiratory gating/triggering. These advanced imaging capabilities and techniques are being used to perform clinical neonatal MRI examinations on the NICU scanner. Additional system enhancements currently underway include the development of phased-array RF coils and the subsequent use of parallel imaging.

The magnetic field strength 1.5 T is used by the majority of adult-size MRI scanners today. The 3-T scanners are becoming more popular, particularly for applications in the head. Nevertheless, there are limitations to 3-T imaging of the spine, chest and abdomen (e.g., increased artifact susceptibility). There is also an increased risk of tissue heating at 3 T and the number and types of MRI-compatible systems that are

commercially available are more limited. Until a small-footprint 3-T magnet is available and demonstrates superior imaging capabilities, the S/N ratio and tissue contrast at 1.5 T provides sufficient image quality and allows the full spectrum of advanced MRI and MRS techniques to be employed, particularly when used with optimized RF coils.

We believe this NICU MRI platform will be beneficial particularly for the evaluation, clinical management and repeated long-term follow-up of neonates. High-quality MRI examinations of the brain, spine, chest and abdomen were obtained using clinically relevant imaging protocols with comparable scan times. The preliminary imaging results obtained in premature sheep during the first hours of life demonstrate the diagnostic as well as research potential of the neonatal MRI system. The quality of the lung images suggests that the neonatal MRI system will prove beneficial to the evaluation of pulmonary problems associated with prematurity as well as in the investigation of both normal and atypical lung development. Similarly, the high-quality abdominal images offer the possibility of the early diagnosis and clinical management of life-threatening conditions such as necrotizing enterocolitis [39]. Finally, MRI avoids ionizing radiation, making it more suitable for such longitudinal evaluations in a neonate.

Because MR image quality is sensitive to motion, sedation is often required to obtain the necessary image quality in young children. In light of the burgeoning evidence to suggest that sedation in the neonatal population is fraught with inherent risk, including brain apoptosis, apnea and bradycardia, there has been an increased emphasis on performing neonatal MRI examinations without sedation [40–45]. To this end, the feed-and-sleep strategy has been found to be effective in many cases [46]. The objective of this approach is to promote and maintain a sound sleep throughout the MRI examination. To this end, the infant is fed approximately an hour before the examination and swaddled with warm blankets or vacuum bag devices, and the MRI room lights are set to a low level. The potential success of this nonsedation approach further benefits from the inherently lower acoustic noise levels of the NICU scanner.

It is known that sensory stimulation such as acoustic noise can elicit autonomic instability in both term and preterm neonates. Consequently, various forms of ear protection are routinely used at institutions performing neonatal MRI examinations. To date, one study has shown changes in heart rate, blood pressure and oxygen saturation in some babies undergoing MRI [1]. Another study did not show such changes [2], and no serious acoustic noise-related adverse effects have been reported for the neonatal population. Although the NICU MRI scanner is substantially quieter than the conventional MRI systems used for neonatal imaging today, neonate hearing protection is still advisable, and measures to further reduce the acoustic noise for the NICU system are being explored.

Compared to an adult-size whole-body MRI system, the initial capital investment and operating costs are much lower for the NICU MRI unit. This is a direct consequence of its smaller footprint and fringe field, reduced weight and low cryogen consumption. In addition, by performing the MRI examination within the NICU, time and staffing demands (hence technical costs) associated with the transport of neonates out of the NICU are reduced. We anticipate that enabling a state-of-the-art MRI system to be readily available to the neonatal population will have a dramatic positive impact on neonatal medical care and management, leading to fewer complications and shortened hospital stays, hence lowering overall medical costs associated with premature birth. Once the clinical/diagnostic benefit of the NICU MRI system is demonstrated and the new MRI platform gains widespread clinical acceptance, it is expected that reimbursement policies associated with its use will be formulated and solidified. Once established, we believe the NICU MRI system will prove to have great benefit both clinically and economically.

Conclusion

Our preliminary experience using a small-bore 1.5-T MRI system demonstrates its feasibility and potential benefit to neonatal medicine. This novel MRI system has the potential to provide state-of-the-art MRI capabilities to all neonates, including the smallest and sickest who are in greatest medical need. Preliminary experience with the prototype system suggests that that this customized neonatal MRI system in its final form may be a model for future NICU MRI systems.

Acknowledgments The authors thank Drs. Brian D. Coley and Alan S. Brody for their helpful comments and contributions to the preparation of the manuscript. The study was partially funded by the March of Dimes Foundation #6-FY109-235 (M.I.), and the Curosurf lung surfactant used was provided by Chiesi Farmaceutici, Italy.

Conflicts of interest We have no conflicts of interest to declare.

References

1. Philbin MK, Taber KH, Hayman LA (1996) Preliminary report: changes in vital signs of term newborns during MR. AJNR 17:1033–1036
2. Battin M, Maalouf EF, Counsell S et al (1998) Physiological stability of preterm infants during magnetic resonance imaging. Early Hum Dev 52:101–110
3. Taber KH, Hayman LA, Northrup SR et al (1998) Vital sign changes during infant magnetic resonance examinations. J Magn Reson Imaging 8:1252–1256
4. Stokowski LA (2005) Ensuring safety for infants undergoing magnetic resonance imaging. Adv Neonatal Care 5:14–27, quiz 52–54
5. Mathur AM, Neil JJ, McKinstry RC et al (2008) Transport, monitoring, and successful brain MR imaging in unsedated neonates. Pediatr Radiol 38:260–264

6. van Wezel-Meijler G, Leijser LM, de Bruine FT et al (2009) Magnetic resonance imaging of the brain in newborn infants: practical aspects. Early Hum Dev 85:85–92
7. Rutherford M (2002) MRI of the neonatal brain. W.B. Saunders, Philadelphia
8. Merchant N, Groves A, Larkman DJ et al (2009) A patient care system for early 3.0 tesla magnetic resonance imaging of very low birth weight infants. Early Hum Dev 85:779–783
9. Whitby EH, Paley MN, Smith MF et al (2003) Low field strength magnetic resonance imaging of the neonatal brain. Arch Dis Child Fetal Neonatal Ed 88:F203–F208
10. Barkovich AJ (2006) MR imaging of the neonatal brain. Neuroimaging Clin N Am 16:117–135, viii–ix
11. Arthur R (2006) Magnetic resonance imaging in preterm infants. Pediatr Radiol 36:593–607
12. Erberich SG, Friedlich P, Seri I et al (2003) Functional MRI in neonates using neonatal head coil and MR compatible incubator. Neuroimage 20:683–692
13. Bluml S, Friedlich P, Erberich S et al (2004) MR imaging of newborns by using an MR-compatible incubator with integrated radiofrequency coils: initial experience. Radiology 231:594–601
14. Whitby EH, Griffiths PD, Lonneker-Lammers T et al (2004) Ultrafast magnetic resonance imaging of the neonate in a magnetic resonance-compatible incubator with a built-in coil. Pediatrics 113:e150–e152
15. Panigrahy A, Bluml S (2007) Advances in magnetic resonance neuroimaging techniques in the evaluation of neonatal encephalopathy. Top Magn Reson Imaging 18:3–29
16. Prager A, Roychowdhury S (2007) Magnetic resonance imaging of the neonatal brain. Indian J Pediatr 74:173–184
17. Rona Z, Klebermass K, Cardona F et al (2010) Comparison of neonatal MRI examinations with and without an MR-compatible incubator: advantages in examination feasibility and clinical decision-making. Eur J Paediatr Neurol 14:410–417
18. Hirsch W, Sorge I, Krohmer S et al (2008) MRI of the lungs in children. Eur J Radiol 68:278–288
19. Adams EW, Counsell SJ, Hajnal JV et al (2000) Investigation of lung disease in preterm infants using magnetic resonance imaging. Biol Neonate 77(Suppl 1):17–20
20. Krishnamurthy R (2010) Neonatal cardiac imaging. Pediatr Radiol 40:518–527
21. Michael R (2008) Potential of MR-imaging in the paediatric abdomen. Eur J Radiol 68:235–244
22. Rao P (2006) Neonatal gastrointestinal imaging. Eur J Radiol 60:171–186
23. Riccabona M (2006) Imaging neonates – special paediatric edition 2006. Eur J Radiol 60:131–132
24. Dyet LE, Kennea N, Counsell SJ et al (2006) Natural history of brain lesions in extremely preterm infants studied with serial magnetic resonance imaging from birth and neurodevelopmental assessment. Pediatrics 118:536–548
25. Darge K, Anupindi SA, Jaramillo D (2008) MR imaging of the bowel: pediatric applications. Magn Reson Imaging Clin N Am 16:467–478, vi
26. Olsen OE (2008) Practical body MRI – a paediatric perspective. Eur J Radiol 68:299–308
27. Seghier ML, Huppi PS (2010) The role of functional magnetic resonance imaging in the study of brain development, injury, and recovery in the newborn. Semin Perinatol 34:79–86
28. Seghier ML, Lazeyras F, Huppi PS (2006) Functional MRI of the newborn. Semin Fetal Neonatal Med 11:479–488
29. Seghier ML, Lazeyras F, Zimine S et al (2004) Combination of event-related fMRI and diffusion tensor imaging in an infant with perinatal stroke. Neuroimage 21:463–472
30. Simbrunner J, Riccabona M (2006) Imaging of the neonatal CNS. Eur J Radiol 60:133–151
31. Rutherford M, Malamateniou C, Zeka J et al (2004) MR imaging of the neonatal brain at 3 tesla. Eur J Paediatr Neurol 8:281–289
32. Rutherford M, Srinivasan L, Dyet L et al (2006) Magnetic resonance imaging in perinatal brain injury: clinical presentation, lesions and outcome. Pediatr Radiol 36:582–592
33. Miller SP, McQuillen PS, Hamrick S et al (2007) Abnormal brain development in newborns with congenital heart disease. New Engl J Med 357:1928–1938
34. Miller JH, McKinstry RC, Philip JV et al (2003) Diffusion-tensor MR imaging of normal brain maturation: a guide to structural development and myelination. AJR 180:851–859
35. Bartha AI, Yap KR, Miller SP et al (2007) The normal neonatal brain: MR imaging, diffusion tensor imaging, and 3D MR spectroscopy in healthy term neonates. AJNR 28:1015–1021
36. Glass HC, Bonifacio SL, Sullivan J et al (2009) Magnetic resonance imaging and ultrasound injury in preterm infants with seizures. J Child Neurol 24:1105–1111
37. Saunders DE, Thompson C, Gunny R et al (2007) Magnetic resonance imaging protocols for paediatric neuroradiology. Pediatr Radiol 37:789–797
38. Lobo L (2006) The neonatal chest. Eur J Radiol 60:152–158
39. Maalouf EF, Fagbemi A, Duggan PJ et al (2000) Magnetic resonance imaging of intestinal necrosis in preterm infants. Pediatrics 105:510–514
40. Jevtovic-Todorovic V, Hartman RE, Izumi Y et al (2003) Early exposure to common anesthetic agents causes widespread neurodegeneration in the developing rat brain and persistent learning deficits. J Neurosci 23:876–882
41. Beauve B, Dearlove O (2008) Sedation of children under 4 weeks of age for MRI examination. Paediatr Anaesth 18:892–893
42. Allegaert K, Naulaers G (2008) Procedural sedation of neonates with chloral hydrate: a sedation procedure does not end at the end of the acquisition of the images. Paediatr Anaesth 18:1270–1271
43. Koch BL (2008) Avoiding sedation in pediatric radiology. Pediatr Radiol 38(Suppl 2):S225–S226
44. Cote CJ (2010) Safety after chloral hydrate sedation of former preterm and term infants for magnetic resonance imaging: are the data clear? Anesth Analg 110:671–673
45. Etzel-Hardman D, Kapsin K, Jones S et al (2009) Sedation reduction in a pediatric radiology department. J Healthc Qual 31:34–39
46. Windram J, Grosse-Wortmann L, Shariat M et al (2012) Cardiovascular MRI without sedation or general anesthesia using a feed-and-sleep technique in neonates and infants. Pediatr Radiol 42:183–187